Received: 29 October 2024 | Accepted: 2 January 2025

DOI: 10.1002/biof.2158

RESEARCH ARTICLE

Biofactors WILEY

FAM49B drives colorectal cancer progression by stabilizing c-Myc through NEK9 phosphorylation

Chen Lu[1,2] | **Tianyu Liu**[2] | **E. Yimin**[3] | **Lin Miao**[4] | **Chunzhao Yu**[1,2] | **Jianping Zhang**[1,5] | **Xiagang Luo**[1]

[1]Department of General Surgery, The Second Affiliated Hospital of Nanjing Medical University, Nanjing, Jiangsu, China

[2]Department of General Surgery, Sir Run Run Hospital of Nanjing Medical University, Nanjing, Jiangsu, China

[3]Department of General Surgery, The Affiliated Suzhou Hospital of Nanjing Medical University, Suzhou, Jiangsu, China

[4]Medical Centre for Digestive Diseases, The Second Affiliated Hospital of Nanjing Medical University, Nanjing, Jiangsu, China

[5]Department of General Surgery, Xiamen Humanity Hospital, Fujian Medical University, Xiamen, Fujian, China

Correspondence

Xiagang Luo, Department of General Surgery, The Second Affiliated Hospital of Nanjing Medical University, Nanjing, Jiangsu 210011, China.
Email: jssylxg2003@njmu.edu.cn

Jianping Zhang, Department of General Surgery, The Second Affiliated Hospital of Nanjing Medical University, Nanjing, Jiangsu 210011, China.
Email: drzhangjp@njmu.edu.cn

Chunzhao Yu, Department of General Surgery, The Second Affiliated Hospital of Nanjing Medical University, Nanjing, Jiangsu 210011, China.
Email: chunzhaoyu@njmu.edu.cn

Funding information

Jiangsu Provincial Commission of Health and Family Planning, Grant/Award Number: Z201603; Science and Technology Development Fund of Nanjing Health and Family Planning Commission, Grant/Award Number: YKK16233; Youth talent support program of Nanjing City during the 13th Five-Year Plan Period, Grant/Award Number: QRX17107

Abstract

Colorectal cancer (CRC) ranks as the third most prevalent cancer globally and is the second leading cause of cancer mortality. FAM49B, a member of the FAM49 gene family, is a recently identified, evolutionarily conserved gene. Emerging studies indicate that FAM49B plays a role in various cancers, though its specific mechanism in CRC remains largely unexplored. In this study, we observed that FAM49B was abnormally expressed in CRC tissues and cell lines, with elevated expression correlating with poor patient prognosis. FAM49B knockdown markedly suppressed CRC cell proliferation by arresting the cell cycle and reducing cell migration and invasion. Single-cell RNA-seq (ScRNA-seq) analysis revealed that high FAM49B expression in malignant epithelial cell clusters was strongly linked to c-Myc oncogene activation. Further, FAM49B knockdown significantly reduced c-Myc expression by enhancing its K48 ubiquitination. We identified NEK9 as a direct interacting partner of FAM49B, with FAM49B knockdown inhibiting NEK9-Thr210 phosphorylation. Similarly, high NEK9 expression was linked to unfavorable prognosis in CRC. In FAM49B-overexpressing CRC cells, NEK9 knockdown significantly suppressed c-Myc expression, c-Myc-ser62 phosphorylation, and reduced cell proliferation, migration, and invasion. Thus, directly targeting the FAM49B/NEK9/c-Myc pathway presents a promising therapeutic approach for c-Myc positive CRC patients.

KEYWORDS

c-Myc, colorectal cancer, FAM49B, NEK9

Chen Lu and Tianyu Liu contributed equally to this study.

1 | INTRODUCTION

Colorectal cancer (CRC) ranks as the third most prevalent cancer globally and the second leading cause of cancer mortality. Global CRC incidence is projected to rise to 2.5 million new cases by 2035.[1] Comprehensive treatments, including surgical resection, have significantly improved CRC survival rates, with a five-year survival rate of up to 72% in patients diagnosed and treated early.[2] However, five-year survival drops to about 50% for advanced CRC and only 12% for metastatic cases, largely due to recurrence and metastasis.[3]

The FAM49 gene family, recently identified and highly conserved through evolution, remains largely unstudied.[4] Current studies suggest that FAM49 genes mainly regulate cell movement in non-tumor cells.[5] As a FAM49 family member, FAM49B is upregulated in multiple sclerosis[6] and may support immune monitoring in mice.[7] Recent research shows FAM49B's involvement in tumor proliferation, invasion, and metastasis,[8,9] hinting at its role in cancer progression, though the exact mechanisms are unclear.

In this study, we found FAM49B expression increased in CRC tumor tissues, with elevated levels closely linked to poor patient prognosis. Functional assays revealed that FAM49B promotes CRC cell proliferation, migration, and invasion, indicating its role in CRC progression. Single-cell RNA-seq (ScRNA-seq) analysis identified malignant epithelial cell clusters with high FAM49B expression as enriched for c-Myc oncogene activation. We further showed that FAM49B stabilizes and activates c-Myc by binding to NEK9, which is also overexpressed in CRC and significantly promotes CRC progression. C-Myc, a prominent Myc family oncogene, is highly expressed across human tumors and essential for tumor cell invasion,[10–14] anchorage-dependent,[15–17] and -independent colony formation[18,19] and metastasis.[20–24] C-Myc has a short half-life, with stability regulated by phosphorylation. Ser62 phosphorylation stabilizes and activates c-Myc,[25,26] whereas Thr58 phosphorylation promotes its degradation.[27–29] We confirmed the existence of the FAM49B/NEK9/c-Myc regulatory axis in CRC cells, highlighting its potential as a promising therapeutic target in CRC.

2 | MATERIALS AND METHODS

2.1 | Bioinformatic analysis

GEPIA database (http://gepia.cancer-pku.cn/) that integrates the resources from TCGA and GTEx projects[30] was used to analyze the differential expression of FAM49B between tumor tissues and normal tissues. Pearson correlation analysis of FAM49B and c-Myc in CRC was also used in the GEPIA database.

The single-cell RNA sequencing (scRNA-seq) dataset was downloaded from the Gene Expression Omnibus (GEO), accession number GSE245552, including 20 samples from 15 colorectal cancer (CRC) patients (16 primary tumor samples and 4 normal colon samples). Data preprocessing was performed using Seurat v4.4.0,[31] where raw expression values were read via the Read10X function and processed into Seurat objects with the CreateSeuratObject function (min.cells = 5, min.features = 300). Cells retained for analysis met the following criteria: gene count per cell between 300 and 6000, mitochondrial gene expression <50% UMIs, ribosomal gene expression <20% UMIs, and UMI count >1000, excluding the top 3% of cells by UMI count. Low-quality cells were filtered, and doublets were removed using DoubletFinder (v2.0.4),[32] assuming a 5% doublet rate. To address batch effects, Harmony (v1.2.0) was used for integration,[33] with clustering performed using FindClusters (resolution = 0.4) into 14 clusters with the top 20 principal components. Clusters were visualized with UMAP, and cell types were annotated into 8 primary types using cell marker genes identified with FindAllMarkers. For epithelial subpopulations, CNV analysis was conducted with inferCNV (v1.3.3),[34] using myeloid cells as reference. Pathway enrichment was analyzed using GSVA (v1.5.0) for Hallmark pathways, and differences were assessed with limma (v3.58.1), with pathways having $|t| > 2$ considered significant and visualized with ggplot2.

2.2 | Tissue specimens and clinicopathological data

We collected samples of primary cancer tissues and adjacent tissues (the adjacent tissues were at least 5 cm away from the tumor margin) of 83 patients who underwent colorectal cancer surgery in the Second Affiliated Hospital of Nanjing Medical University from January 2018 to October 2018. This study was approved by the Ethics Committee of the Second Affiliated Hospital of Nanjing Medical University (No.2020KY092) in accordance with the Declaration of Helsinki. All participants signed informed consent.

The basic clinical information of 83 patients was collected and the patients were followed up once every 3 months in the first 2 years after operation and once every 6 months in the third to fifth years after operation punctually. Follow-up data included medical history, chest and abdomen CT, electronic colonoscopy, and

CEA. Follow-up forms were outpatient follow-up and telephone follow-up. The last follow-up time was September 19, 2023, and the total follow-up time of each patient was at least 5 years.

2.3 | Kaplan–Meier survival analysis

Kaplan–Meier survival analysis of disease-specific survival (DSS) were implemented by using the cohort of 83 patients. The hazard ratio (HR) and log-rank *p*-value were automatically calculated between the two groups. The graphs were plotted using GraphPad Prism (Version 8.0).

The cBioPortal database (http://www.cbioportal.org/) hosts omics data from large alliances (including integrated TCGA databases, GEO databases, etc.) and publications from individual laboratories. In this database, we selected a colorectal cancer dataset (TCGA, PanCancer Atlas) containing 594 samples to analyze the prognostic value of FAM49B in DSS of CRC patients. The COAD dataset from the GEPIA database was used to analyze the value of NEK9 in the overall survival (OS) of CRC patients.

2.4 | Cell lines and cell culture

The human CRC cell lines HCT116, SW480, SW620, DLD1, and CaCO2 were purchased from FuHeng Biotechnology Co., Ltd (Shanghai, China). The human normal colon epithelial cell line NCM460 was presented by the Lab center of the Second Affiliated Hospital of Nanjing Medical University. The cell lines we purchased were cultured according to the instruction manual. NCM460 cell line was maintained in RPMI 1640 medium (Gibco, MD, USA) with 10% fetal bovine serum (Vazyme, Nanjing, China).

2.5 | Transient transfection and lentiviral infection

Small interference RNA (siRNA) specifically targeting FAM49B or NEK9, and negative control siRNA (si-NC) were acquired from Proteinbio Corporation (Nanjing, China). The plasmids respectively expressing FAM49B with Flag-tag and expressing NEK9 with HA-tag were obtained from MIAOLING Biology Corporation (Wuhan, China). Lipofectamine 3000 (Invitrogen, Carlsbad, USA) was used to transfect a specified amount of RNA or plasmid into cells when cells grew to a confluency of 50%–70%, according to the manufacturer's protocols. The sequences of siRNAs are listed as follows: siFAM49B #1, 5′-GCAGGCUCUUGCUAAACAGUUTT-3′; siFAM49B #2, 5′-AUCCUGCCAUACAGAAUGAUUTT-3′; siFAM49B #3: 5′-GCAGCUAAUUAUGCAUUGCAUTT-3′; NEK9 siRNA #1, 5′-GCAGAAGUUGAACAAGAAAT-3′; NEK9 siRNA #2, 5′-GCUCUGAUAUCUGUACCUCAUTT-3′; NEK9 siRNA #3, 5′-CCCACUUAACCUGUGUGUGAATT-3′; si-NC, 5′-UUCUCCGAACGUGUCACGUTT-3′.

The siRNA sequence with the highest efficiency was cloned into the PGMLV-mScarlet-puro vector to construct lentivirus. For lentiviral infection, the lentivirus was diluted in the medium with fetal bovine serum to the desired concentration, and polybrene was added in it to enhance the efficiency of infection.

2.6 | CCK-8 assay

After cells were transfected for 48 h, we used serum-free medium or medium with 1% serum to prepare cell suspension. Next, around 2,000 cells per well were seeded into 96-well plates and then were cultured with a medium containing 10% serum after about 24 h. Subsequently, 10μLCell Counting Kit-8 (CCK-8, Vazyme) reagent was added to each well at 0, 24, 48, 72, and 96 h. The absorbance of cells was measured using a microplate spectrophotometer (BioTek, USA) at 450 nm.

2.7 | EdU incorporation assay

Similarly, the cell suspension containing around 20,000 cells per well with serum-free medium was seeded into 48-well plates. After waiting for around 24 h, we replaced the medium each well with medium involving 10% serum. When cells grew to a confluency of 80%, Edu was added to each experimental well and incubated with cells for 2 hours. Then, 4% polyformaldehyde was used to fix cells for 30 min at room temperature. Next, cells were permeabilized with 0.3% Triton X-100 for 15 min. Edu reactive solution was prepared according to the instruction and was used to incubate cells for 30 min in the dark. At last, the nucleus of cell was stained with 4′,6-diamidino-2-phenylindole (DAPI) for 10 min, and then each well was imaged with the fluorescence microscopy in a dark area. The Edu reagent kit was purchased from Beyotime Biotechnology.

2.8 | Flow cytometry assay

The cells were harvested with 0.25% Trypsin–EDTA and washed with ice-cold PBS. Then, precooled 75% ethanol

solution was used to fix cells overnight at 4°C. After washing the cells with PBS twice, we used an appropriate amount of propidium iodide staining solution to incubate cells for 30 minutes in the dark. The cell cycle was evaluated by flow cytometry (BD Biosciences).

2.9 | Transwell assay

For Transwell migration assay, the cells were collected in serum-free medium, and seeded in the upper chamber (Corning, NY, USA) at the concentration of 8×10^5/mL. and then 0.75 mL medium with 10% serum was put in the lower chamber. After around 24 h, the migrated cells were fixed with 4% polyformaldehyde for 30 min at room temperature, and then were stained with 0.1% crystal violet for 20 min in the dark. Next, the chamber was washed with pure water and was dried followed by imaging. To evaluate the invasive ability of cells, the bottom of the upper chamber was coated with diluted Matrigel (Corning) before the collection of treated cells. All the next procedures are the same as described above.

2.10 | RNA isolation and real-time quantitative PCR (RT-qPCR)

The total RNA was extracted from each tissue sample stored at −80°C and cell samples using TRIzol® reagent (Invitrogen, Carlsbad, CA, USA) and SteadyPure RNA Extraction Kit (Accurate Biology, Hunan, China, #AG21024). The concentration and quality of RNA were assessed using a One Drop OD-1000 spectrophotometer, with an A260/280 ratio within the range of 1.8–2.0. Then, 1000 ng of RNA was converted into cDNA in a 20 μL reaction mixture by using Hiscript III Reverse Transcriptase (Vazyme, Nanjing, China). The reaction procedure of reverse transcription was set to 50°C for 15 min and 85°C for 5 s. RT-qPCR was performed using a LightCycler 480 Real-time PCR Detection System (Roche, Switzerland) and ChamQ Universal SYBR qPCR Master Mix (Vazyme), following the manufacturer's protocol. The gene-specific primers are listed as follows: GAPDH-Forward, 5′-TCAACGGATTTGGTCGTATTG-3′; GAPDH-Reverse, 5′-TGGGTGGAATCATATTGGAAC-3′; FAM49B-Forward, 5′-CTCAAGATGACAAATCCTGC-3′; FAM49B-Reverse, 5′-CCGGTACATTGTTAATCCTC-3′; NEK9-Forward, 5′-AAGCTATCCGTCAGGTGTCA-3′; NEK9-Reverse, 5′-GTTTCGTGTCAGAACCACCA-3′; c-Myc-Forward, 5′-GAACAAGAAGATGAGGAAGAA-3′; c-Myc-Reverse, 5′-CAGAAGGTGATCCAGACT-3′.

2.11 | Western blot

Total protein was extracted from gastric cancer cells or tissues with RIPA lysis buffer (Beyotime, Shanghai, China) containing 1% PMSF. Then protein concentration was determined using BCA reagent kit (Vazyme). Ten to twenty micrograms of protein samples were separated by 10%–12.5% SDS-PAGE gel System (Bio-Rad) and transferred to polyvinylidene difluoride membranes (Millipore). The membranes were blocked with 5% non-fat milk or 5% BSA for 2 h at room temperature and subsequently were incubated overnight at 4°C with the following primary antibodies: β-actin (Sigma, #5441, 1:5000), GAPDH (Abcam, ab8245, 1:5000), FAM49B (Santacruz, sc-390478, 1:1000), c-Myc (Abcam, ab32072, 1:1000), phospho-c-Myc (S62) (Abcam, ab185656, 1:1000), cyclinD1 (Proteintech, 26939-1-AP, 1:5000), cyclinE1 (Proteintech, 11554-1-AP, 1:1000), E-cadherin (Abcam, ab40772, 1:5000), N-cadherin (Abcam, ab76011, 1:5000), Vimentin (Proteintech, 10366-1-AP, 1:5000), NEK9 (Proteintech, #11192-1-AP, 1:3000), phospho-NEK9 (Thr210) (Abcam, #ab63553, 1:1000), Flag (Sigma, #F1804, 1:5000), and HA (Sigma, #H9658, 1:5000). Next, the membranes were incubated with goat anti-rabbit IgG (SAB, #L3012, 1:5000) or goat anti-mouse IgG (SAB, #L3032, 1:5000) for an hour at room temperature and then were washed with Tris-buffered saline-tween 20 (TBST) three times for half an hour. Finally, the protein bands were imaged and analyzed with ECL Chemiluminescence Kit (Vazyme) and Image J software.

2.12 | Animal studies

All animal experiments were approved by the Institutional Animal Care and Use Committee (IACUC) at Nanjing Medical University (No. IACUC-2410083), and their procedures were conducted in accordance with the guidelines of the Animal Care and Use Committee Guidelines. Male BALB/c nude mice (4–6 weeks old) were purchased from GemPharmatech Co. Ltd. (Nanjing, China).

For the subcutaneous xenograft model, SW480 cells with negative control (NC) or FAM49B knockdown (FAM49B-KD) lentivirus were adjusted to 1×10^7/mL. 200 μL of cell suspension was subcutaneously injected into the left axilla of each mouse. The tumor size of each mouse was measured every week. Their subcutaneous tumor tissues were collected for weighting and volume measurement when all mice were euthanized. The tumor volume was calculated using the formula of $(\text{width}^2 \times \text{length})/2$.

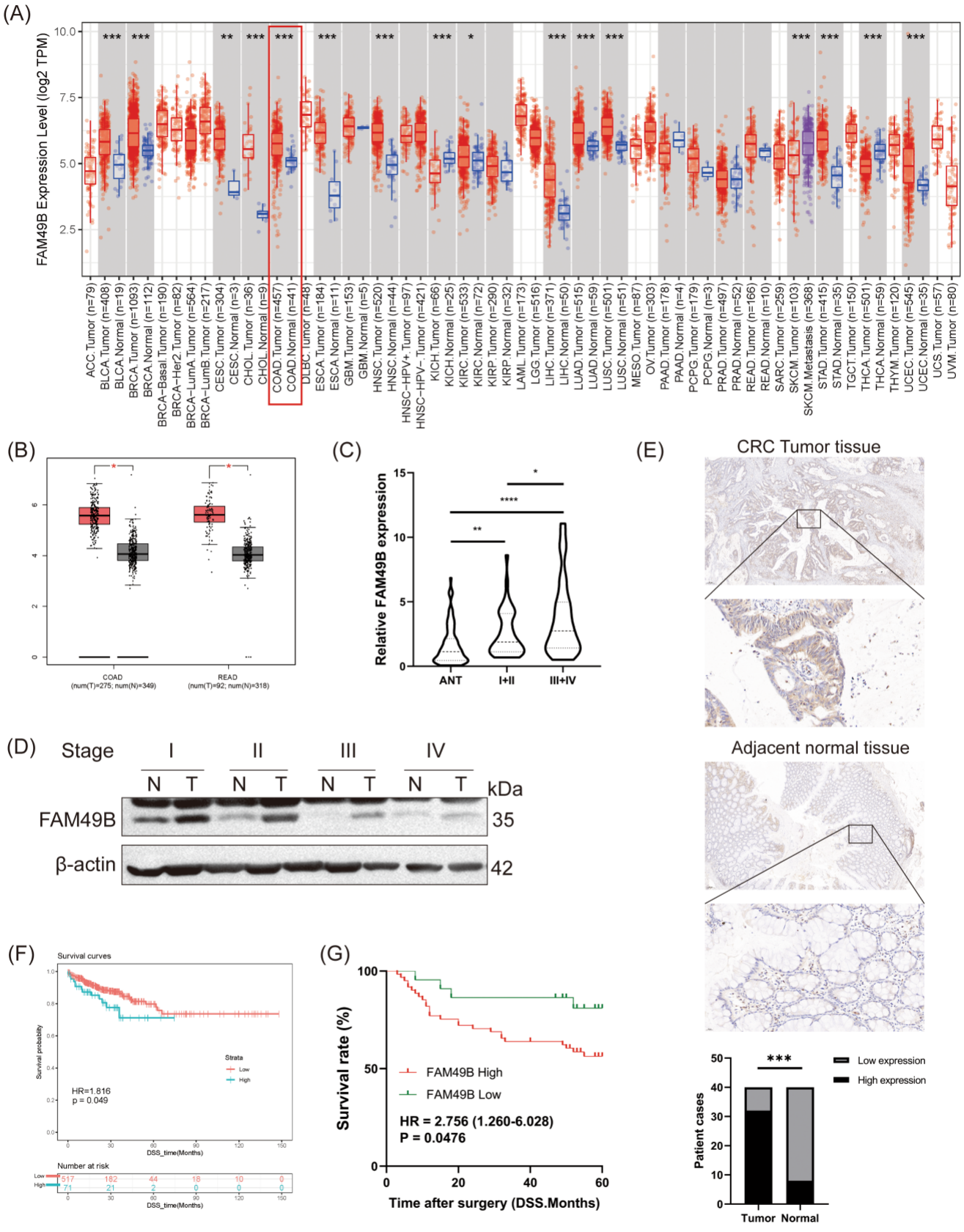

FIGURE 1 Legend on next page.

TABLE 1 The relationship between FAM49B expression and clinicopathological characteristics ($n = 83$).

Characteristics	FAM49B expression		*p* value
	High ($n = 61$)	Low ($n = 22$)	
Age			0.073
<60 years old	33	7	
≥60 years old	28	15	
Gender			0.551
Male	35	11	
Female	26	11	
Stage			0.020*
I–II stage	24	15	
III–IV stage	37	7	
T stage			0.439
T1–T2	33	14	
T3–T4	28	8	
N stage			0.040*
N0	26	15	
N1–2	35	7	
M stage			0.289
M0	58	22	
M1	3	0	
CEA			0.016*
≥5 ng/mL	45	10	
<5 ng/mL	16	12	
Postoperative tumor recurrence			0.017*
Recurrence	22	2	
No recurrence	39	20	
Postoperative tumor metastasis			0.031*
Metastasis	20	2	
No metastasis	41	20	

FIGURE 1 The expression level of FAM49B increased in colorectal cancer and was significantly correlated with patient prognosis. (A) The expression level of FAM49B mRNA in various malignant tumor tissues and corresponding normal tissues in the TCGA database. (B) Expression levels of FAM49B mRNA in colorectal cancer tissues from COAD dataset, READ dataset in TCGA database, and in normal colorectal tissues including GTEx database. (C) The expression level of FAM49B mRNA in colorectal cancer tissues and adjacent normal tissues. (D) The expression level of FAM49B protein in colorectal cancer tissues and adjacent normal tissues. (E) FAM49B immunohistochemical positive and negative tumor tissue sections, normal tissue sections adjacent to cancer. And bar plot of corresponding statistical analysis was performed. The scale was 100 μm, and the enlarged scale is 20 μm. (F, G) Kaplan–Meier survival curves were used to compare the DSS survival time of patients with high and low FAM49B expression: (F) 589 cases of TCGA colorectal cancer adenocarcinoma in cBioportal database; (G) 83 patients with colorectal cancer from the Second Affiliated Hospital of Nanjing Medical University. ANT, normal adjacent tissue; COAD, colon cancer dataset; DSS, disease-specific survival; READ, rectal cancer data set. *$p < 0.05$, **$p < 0.01$, ***$p < 0.001$, ****$p < 0.0001$.

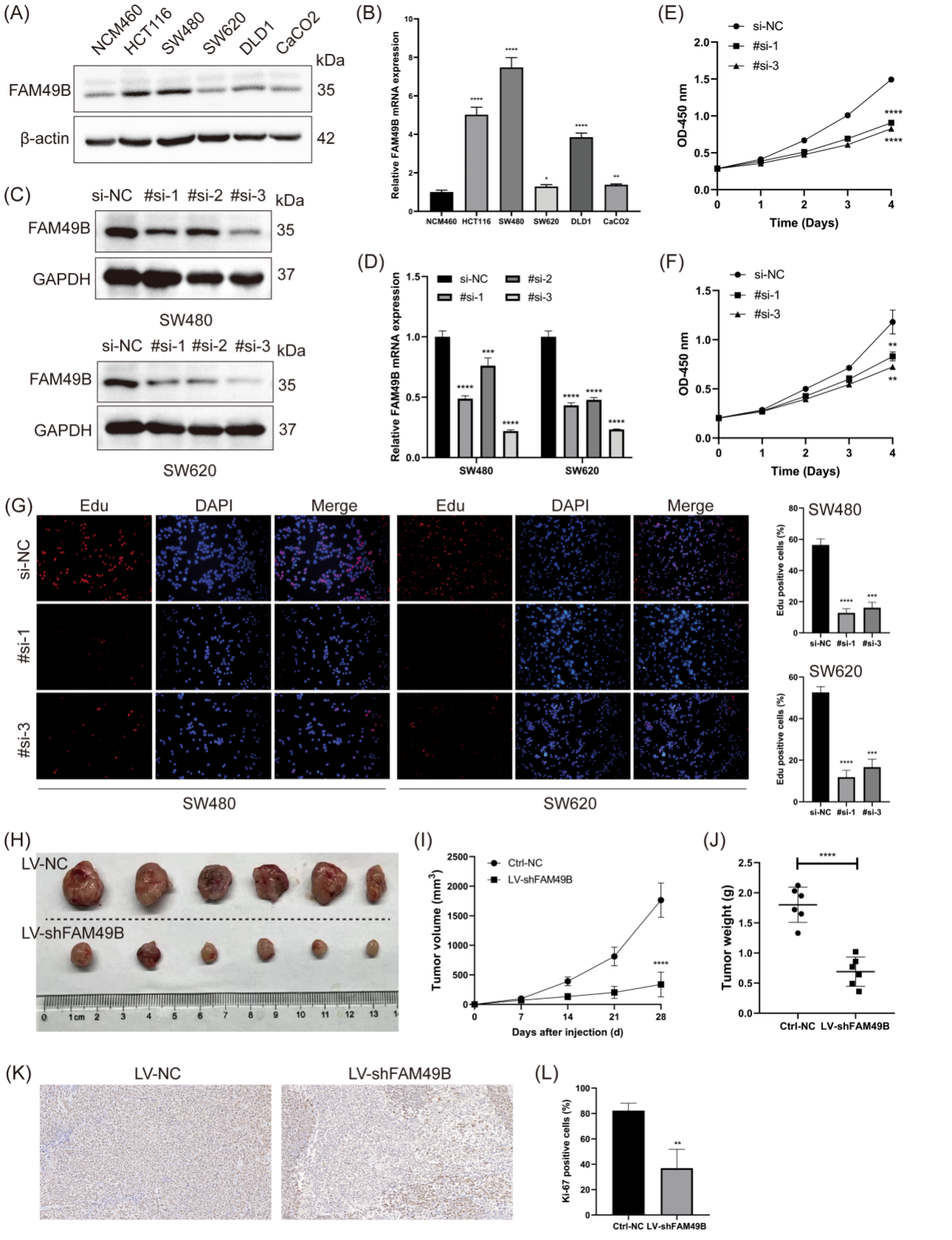

FIGURE 2 Legend on next page.

For the tumor metastasis model, 100 μL of cell suspension with NC or FAM49B-KD lentivirus was slowly injected into their tail vein to construct the lung metastasis model. After about 30 days, tumor metastasis burden of each mouse was evaluated using in vivo imaging technology. Then, all mice were euthanized, and their lungs were dissected and isolated and then fixed in 4% paraformaldehyde for further analysis of hematoxylin and eosin (H&E) staining.

2.13 | CO-IP assay

Cell protein was extracted using IP lysis buffer and then was incubated with the primary antibody or IgG overnight at 4°C. Next day, the mixture was incubated with protein A/G magnetic beads (#88802, Thermo Scientific) at room temperature for 2 h. After washing beads three times, bound proteins were eluted and analyzed by western blotting as indicated.

2.14 | Interactome analysis by immunoprecipitation-mass spectrometry (IP-MS)

Protein complexes were isolated from cell lysates using antibody-based immunoprecipitation. Samples were thawed and fractionated into approximately 1 cm strips, which were then cut into smaller segments. Each sample was washed with distilled water, followed by decolorization with 30% acetonitrile (ACN) in 50 mM ammonium bicarbonate for 4–8 h at room temperature. After decolorization, samples were dehydrated with 100% ACN until the colloidal particles turned white. Proteins were reduced with 10 mM dithiothreitol (DTT) in 50 mM ammonium bicarbonate, alkylated with 20 mM iodoacetamide (IAA), and digested with trypsin overnight at 37°C. The resulting peptides were extracted and dried for subsequent LC–MS/MS analysis. Peptides were dissolved in 0.1% formic acid (FA) and analyzed on a high-resolution Q Exactive HF-X mass spectrometer (Thermo Fisher Scientific) using a data-dependent acquisition (DDA) mode. Proteome Discoverer software was used for data processing, with peptide and protein false discovery rates controlled below 1%. Strict criteria were applied to screen for interacting proteins: (i) a differential $\log_2$ fold-change ($\log_2$FC) >1.5 between IP and IgG groups within each group and (ii) a sum PEP (Posterior Error Probability) score exceeding 50 points for interaction confidence.

2.15 | c-Myc ubiquitination assay

Control and FAM49B-KD cells were treated with 10 μM MG132 (MCE, Shanghai, China) for 6 h before cell lysis. Then, the following steps are consistent with CO-IP assay, except that an anti-c-Myc antibody (Proteintech, #10828-1-AP, 1:100) was used.

2.16 | Hematoxylin and eosin (H&E) staining and immunohistochemistry (IHC)

HE staining and IHC staining were performed as previously described.[35] Briefly, for HE staining, tissue sections were deparaffinized and rehydrated, followed by staining with hematoxylin for 5 min and eosin for 2 min. For IHC assay, tissue sections underwent antigen retrieval in citrate buffer (pH 6.0) at 95°C for 20 min. Endogenous peroxidase activity was blocked with 3% hydrogen peroxide, and nonspecific binding was inhibited using 5% BSA. The sections were then incubated with the anti-FAM49B antibody (Santacruz, sc-390478, 1:100) and secondary antibody, followed by staining with 3,3′-diaminobenzidine (DAB). Data analysis was assisted by the Department of Pathology, the Second Affiliated Hospital of Nanjing Medical University.

FIGURE 2 FAM49B promotes the proliferation ability of CRC cells. (A) Western blot analysis in normal colon epithelial cells NCM460, human colorectal cancer cell lines HCT116, SW480, SW620, DLD1, and CaCO2 relative expression levels. (B) qRT-PCR was used to detect the relative expression level of FAM49B mRNA in normal colon epithelial cells NCM460, human colorectal cancer cell lines HCT116, SW480, SW620, DLD1, and CaCO2. (C) Western blot analysis of the knockdown efficiency of FAM49B protein in SW480 and SW620 cells. (D) The knockdown efficiency of FAM49B mRNA in SW480 and SW620 cells was detected by qRT-PCR. (E, F) CCK-8 detected the proliferation function of SW480 and SW620 cells. (G) Edu was used to detect the proliferation function of SW480 and SW620 cells with a scale of 100 μm. (H) Representative image of tumorigenesis after SW480 cells with NC or LV-shFAM49B were injected into the armpit skin of nude mice. (I) Changes of subcutaneous tumor volume in each group with time. (J) The weight of subcutaneous tumors in each group of nude mice. (K, L) Ki-67 levels in subcutaneous tumors of nude mice in each group were analyzed by immunohistochemical staining with a scale of 100 μm. *s*$p < 0.01$, ***$p < 0.001$, ****$p < 0.0001$.

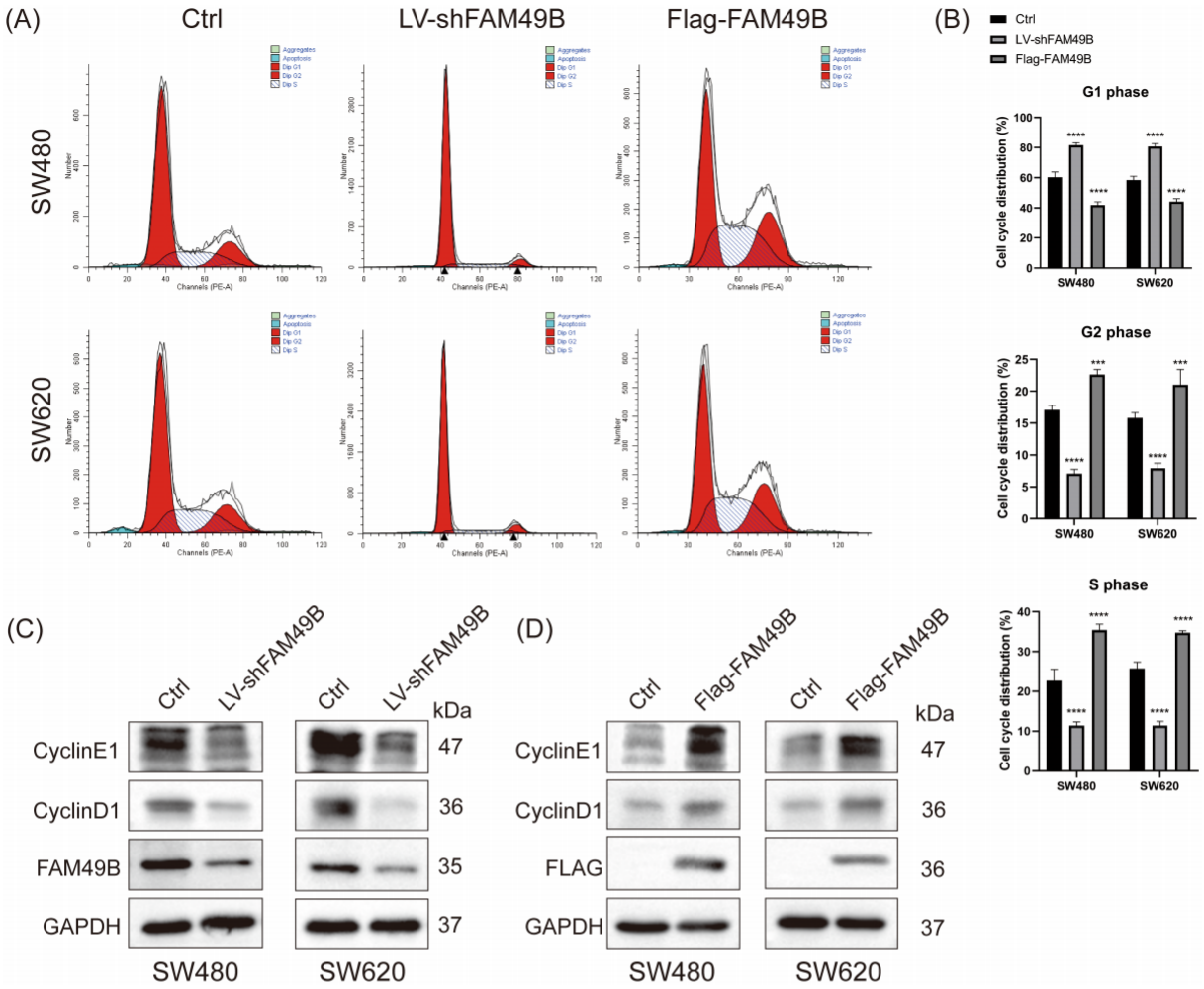

FIGURE 3 Effect of FAM49B on the cell cycle of SW480 and SW620. (A) After successful knockdown of FAM49B and overexpression of FAM49B, the effect of SW480 and SW620 cell cycle was detected by flow cytometry. (B) Bar plot of the corresponding statistical analysis was performed. (C, D) Western blot analysis of cyclinD1 and cyclinE1 expression in SW480 and SW620 cells with FAM49B knockdown (C) or FAM49B overexpressed (D). ***$p < 0.001$, ****$p < 0.0001$.

2.17 | Immunofluorescence (IF)

Experimental cells were seeded into a 24-well plate overnight, followed by fixing with 4% formaldehyde at room temperature for 15 min. Then, the fixed cells were permeabilized by 0.1% Triton X-100 at room temperature, followed by blocking in normal goat serum for half an hour. The anti-FAM49B antibody (1:50) and anti-NEK9 antibody (1:100) were added to the blocked cells for overnight incubation with shaking at 4°C. The next day, the cells were incubated in secondary antibodies with DAPI at room temperature for 1 h. Finally, the stained cells were imaged with fluorescence microscopy in a dark area.

2.18 | Statistical analysis

Statistical analysis was performed with R (v4.2.2), GraphPad Prism (Version 8.0), and SPSS software (Version 23.0). Independent sample *t*-test was used for continuous variable comparison between the two groups, and χ^2-test was used for classified variable comparison. All *t*-tests were bilateral, and $p < 0.05$ showed significant statistical difference. To ensure robustness, all experiments were repeated at least three times independently, unless stated otherwise.

3 | RESULTS

3.1 | Increased FAM49B expression in CRC and its prognostic significance

Pan-cancer analysis using the TCGA database revealed significant FAM49B overexpression in various cancers, notably within digestive system tumors (Figure 1A). In the TCGA COAD and READ datasets, representing colon and rectal cancers, FAM49B expression was markedly

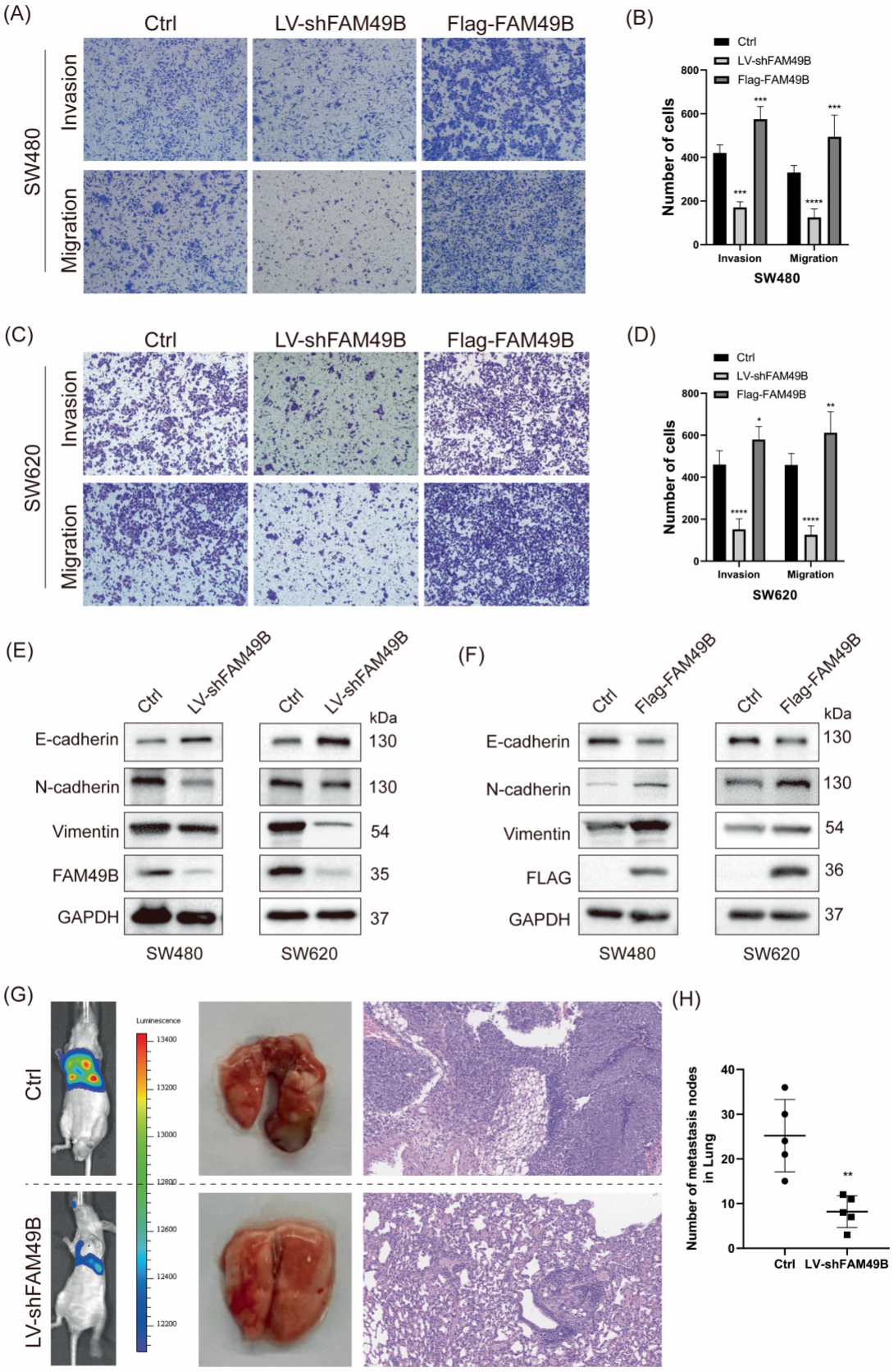

FIGURE 4 Legend on next page.

elevated (Figure 1B). To verify FAM49B expression in CRC tissues, we analyzed paired tumor and adjacent normal tissues from 83 CRC patients who underwent surgery, alongside their clinical data. The qRT-PCR and western blot results indicated significantly higher FAM49B expression in CRC tissues compared to adjacent normal tissues (Figure 1C,D). Immunohistochemical analysis of a random sample of 40 patients' tissues showed that 80% (32/40) of CRC samples were positive for FAM49B expression (Figure 1E). Based on qRT-PCR results, we classified the 83 patients into high-expression (73.49%, 61/83) and low-expression (26.51%, 22/83) groups. We statistically analyzed clinical parameters including age, sex, tumor pathology stage, TNM stage, preoperative CEA levels, and postoperative progression (recurrence and metastasis) (Table 1). FAM49B expression did not correlate significantly with age, sex, or tumor T stage ($p > 0.05$) but was significantly associated with tumor stage ($p = 0.020$), lymph node metastasis ($p = 0.040$), and postoperative progression (recurrence: $p = 0.017$; metastasis: $p = 0.031$). Kaplan–Meier survival analysis indicated that high FAM49B expression is a risk factor for disease-specific survival (DSS) (Figure 1G). Analysis of 589 TCGA colorectal cancer cases in the cBioPortal database confirmed our findings, showing significant correlation between high FAM49B expression and poorer DSS (Figure 1F).

3.2 | FAM49B promotes the proliferative capacity of SW480 and SW620 cells

We measured FAM49B expression levels in the normal colon cell line NCM460 and CRC cell lines HCT116, SW480, SW620, DLD1, and CaCO2 using qRT-PCR and western blot. Compared to NCM460, FAM49B mRNA and protein levels were significantly elevated in CRC cell lines, with SW480 showing the highest and SW620 showing lower expression (Figure 2A,B). Consequently, we selected SW480 and SW620 cell lines for subsequent experiments. We designed three small interfering RNAs (siRNAs: #si-1, #si-2, #si-3) to knock down FAM49B and confirmed their efficiency using qRT-PCR and western blot. The siRNA #si-3 demonstrated the highest knockdown efficiency in both SW480 and SW620 cells (Figure 2C,D). This sequence was then packaged into plasmid and lentivirus to establish stable FAM49B knockdown lines for SW480 and SW620 cells.

To assess the impact of FAM49B on CRC cell proliferation, we performed CCK-8 and Edu assays on SW480 and SW620 cells post-FAM49B knockdown. Results indicated a significant reduction in the proliferation capacity of SW480 and SW620 cells following FAM49B knockdown (Figure 2E–G). In addition, FAM49B overexpression enhanced the proliferative activity of CRC cells (Figure S1). To confirm in vivo effects, we injected SW480 cells with stable FAM49B knockdown subcutaneously into nude mice and monitored tumor growth weekly for 4 weeks. FAM49B-knockdown tumors showed slower growth over time, maintaining smaller, and uniform volumes (Figure 2H,I). Tumor weight was also significantly reduced compared to the normal control group (LV-NC) (Figure 2J). Ki-67 IHC staining showed significantly reduced Ki-67 levels in FAM49B-knockdown tumors versus controls, indicating suppressed cell proliferation (Figure 2K,L).

3.3 | FAM49B facilitates cell cycle progression of SW480 and SW620 cells

Cell proliferation depended on the stable process of the cell cycle. Based on the above results, the effect of FAM49B on the cell cycle of CRC was further detected. Compared with the control group, there was a significant decrease in the percentage of SW480 and SW620 cells in G1 phase and a significant increase in S phase after stable knockdown of FAM49B. Conversely, overexpression of FAM49B significantly decreased the percentage of the cells in G1 phase and significantly increased the percentage in S phase and G2 phase (Figure 3A,B). These results mean FAM49B knockdown could induce cell cycle arrest in the G1 phase of SW480 and SW620 cells.

According to the results of the flow cell cycle, western blot experiment was used to further detect the expression changes of G1/S phase-related proteins cyclinD1 and cyclinE1. The results in turn verified the conclusion of flow cell cycle, that is, the expressions of cyclinD1 and cyclinE1 in SW480 and SW620 cells were significantly decreased after FAM49B was knocked down, while the

FIGURE 4 FAM49B promotes the invasion and migration abilities of CRC cells. (A, C) The invasion and migration conditions of treated SW480 and SW620 cells were measured by Transwell assay. (B, D) Statistical significance was analyzed according to the number of invaded and migrated cells. (E, F) The protein expression levels of E-cadherin, N-cadherin, and vimentin in the sw480 and sw620 cells were examined by western blot. (G, H) Live imaging analysis of nude mice in each group, HE staining detected the number of tumor nodules in the lung and corresponding statistical analysis. The scale is 100 μm. * < 0.05, **$p < 0.01$, *** < 0.001, ****$p < 0.0001$.

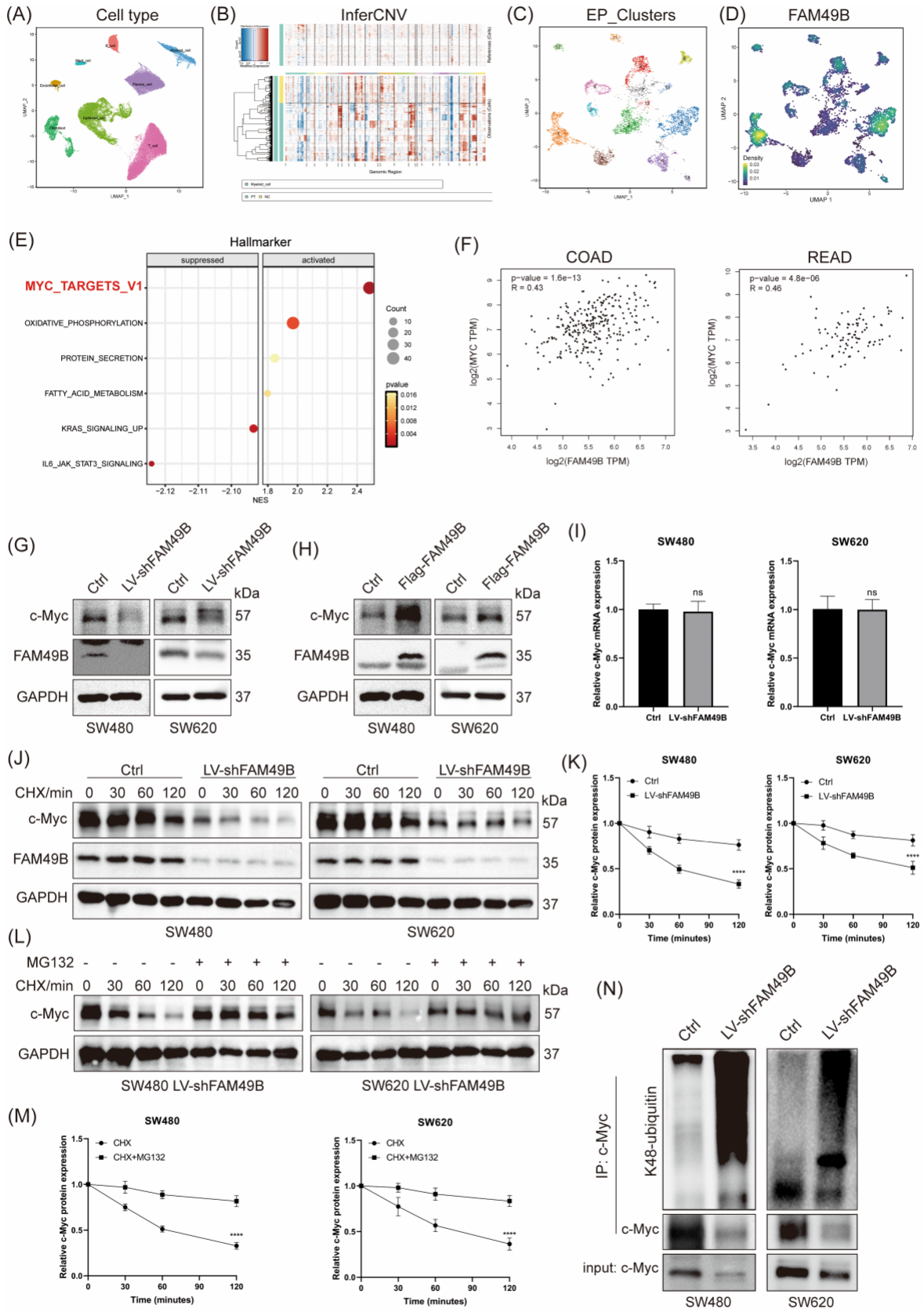

FIGURE 5 Legend on next page.

expressions of cyclinD1 and cyclinE1 were significantly up-regulated after overexpression of FAM49B (Figure 3C,D).

3.4 | FAM49B enhances CRC cell invasion and migration via EMT activation

To investigate the impact of FAM49B on the migratory and invasive abilities of CRC cells, we employed Transwell assay to evaluate their migration and invasion capacities. The results showed that the migration and invasion ability were inhibited after stable knockdown of FAM49B, but significantly enhanced after FAM49B overexpression (Figure 4A–D). Epithelial–mesenchymal transition (EMT) played a very important role in the process of tumor cell metastasis. Western blot experiment was used to further detect the expression changes of EMT-related proteins E-cadherin, N-cadherin, and vimentin. The experimental results showed that knocking down FAM49B significantly increased the expression of E-cadherin and decreased the expression of N-cadherin and vimentin, while overexpressing FAM49B significantly increased the expression of N-cadherin and vimentin and decreased the expression of E-cadherin (Figure 4E,F).

To further explore the influence of FAM49B on CRC metastasis, SW480 cells stably knocked down by FAM49B were injected into the tail vein to produce lung metastasis, and the metastasis of tumor cells was observed. Before collecting the lung metastasis samples of nude mice, we performed in vivo imaging detection on all nude mice and found that the visible spectrum of lung metastasis in FAM49B knockout group was significantly lower than that in normal control group. After dissecting nude mice, the lung metastasis was examined by HE staining. The results showed that the number of lung metastases in the FAM49B knockout group was significantly lower than that in the normal control group (Figure 4G,H).

3.5 | FAM49B upregulates the c-Myc oncoprotein and prevents c-Myc from proteasomal degradation

To investigate the potential mechanism of FAM49B in CRC cells, we analyzed publicly available single-cell RNA sequencing data from GSE245552. After performing quality control, filtering out doublets, and correcting for batch effects, 20 samples from 15 patients were further analyzed, containing 71,991 single-cell transcriptomes. Using UMAP clustering and annotating cell type-specific markers, we identified 8 distinct cell clusters, including T cells, B cells, epithelial cells, myeloid cells, fibroblasts, endothelial cells, mast cells, and plasma cells (Figure 5A). To further screen malignant epithelial cells, we used myeloid cells as reference cells to infer copy number variations (CNVs) in all epithelial cells. By using the average CNV score of epithelial cells from normal colon tissues as a threshold, we finally obtained 6247 malignant epithelial cells (Figure 5B). Malignant epithelial cells were then reclustered into 14 clusters, and visualization was performed using UMAP (Figure 5C). It is worth noting that FAM49B was predominantly expressed in cluster 0 and cluster 1 (Figure 5D). Then, GSEA of differential genes between cell clusters with high and low expression of FAM49B identified MYC_-Targets_V1 as the most strongly activated hallmark gene signature (Figure 5E). Correlation analysis also showed that FAM49B and MYC were significantly positively correlated in COAD and READ datasets from GEPIA database (COAD, $R = 0.43$, $p = 1.6E\text{-}13$; READ, $R = 0.46$, $p = 4.8e\text{-}06$. Figure 5F).

Western blot technique was used to detect the expression of c-Myc in SW480 cells and SW620 cells

FIGURE 5 FAM49B upregulates the c-Myc oncoprotein and prevents c-Myc from proteasomal degradation. (A) UMAP plots of scRNA-seq profiled in this study were colored based on cell type. (B) Chromosomal heat maps of inferred CNVs in epithelial cells, with red denoting amplification and blue signifying deletion. (C) UMAP plots of malignant epithelial cells with 14 clusters. (D) UMAP plots of malignant epithelial cells with FAM49B expression. (E) Bubble map of the hallmarks of differential genes between cell clusters with high FAM49B expression and low FAM49B expression using GSEA. (F) Correlation analysis of FAM49B and c-Myc in COAD and READ datasets within GEPIA database. (G, H) Immunoblots of the indicated proteins of total lysates from SW480 and SW620 cells with stable knockdown of FAM49B (G) or overexpressing FAM49B (H), compared with the control group. (I) Relative c-Myc mRNA expression was analyzed by RT-qPCR in SW480 and SW620 cells with stable knockdown of FAM49B, compared with the control group. (J, K) Representative immunoblots (J) and quantification (K) of c-Myc protein levels in total lysates of SW480 and SW620 cells with stable knockdown of FAM49B, compared with the control group, in response to CHX treatment. (L, M) Representative immunoblots (L) and quantification (K) of c-Myc protein levels in total lysates of SW480 and SW620 cells with stable knockdown of FAM49B treated with DMSO or MG132, in the presence of CHX treatment. (N) Immunoprecipitation of c-Myc was obtained from SW480 and SW620 cells in the control group or FAM49B stable knockdown group. K48 and c-Myc were detected by western blot assay with immunoprecipitation products and total lysate.

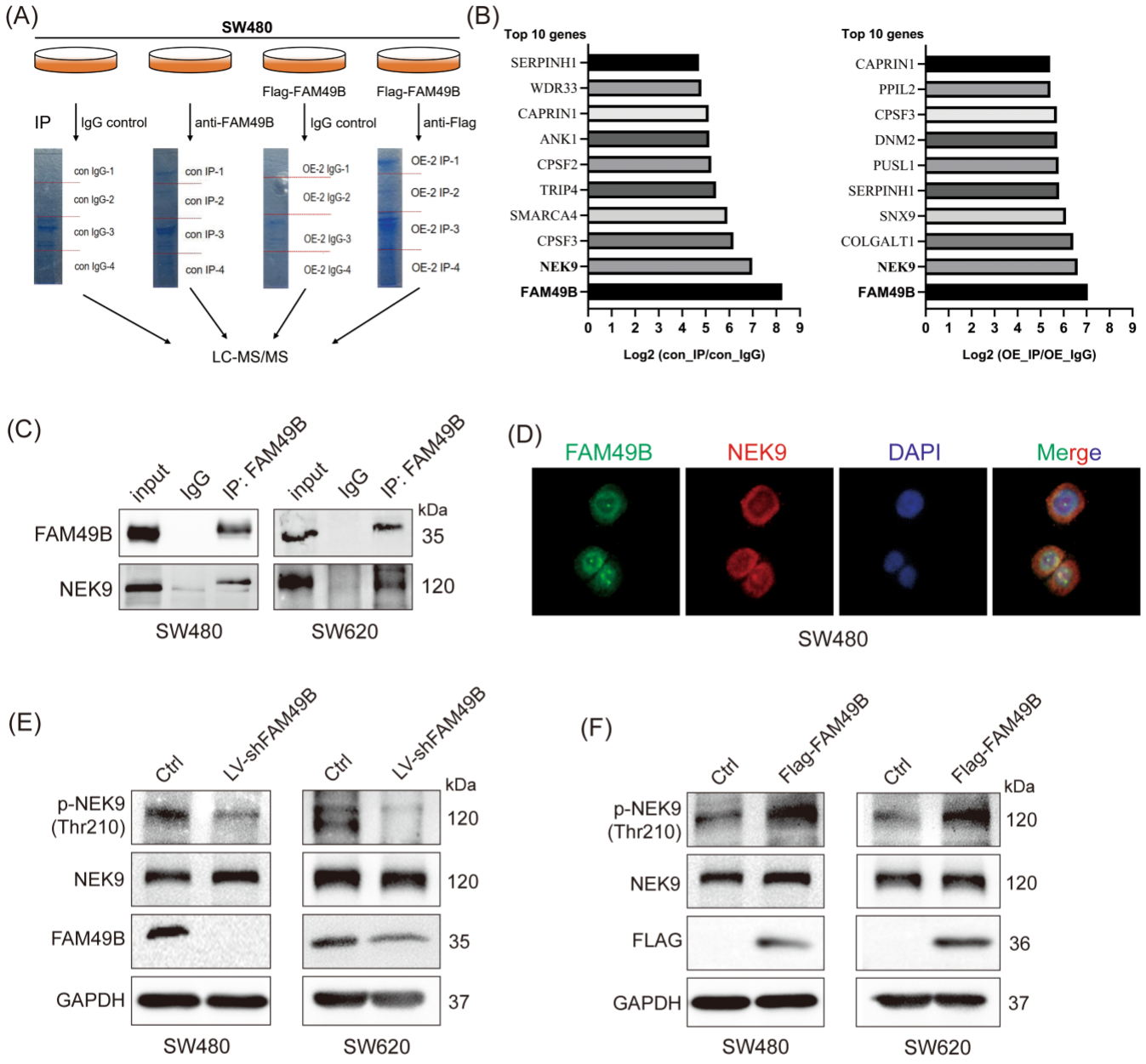

FIGURE 6 FAM49B binds to and activates NEK9. (A) Schematic diagram of IP-MS-based group analysis of protein interactions. (B) The top 10 potential interacting proteins of FAM49B in the normal endogenous FAM49B IP group (left) and the overexpressed exogenous FAM49B Flag IP group (right). (C) CO-IP experiment verified the binding of FAM49B and NEK9 in SW480 cells and SW620 cells. (D) Localization of the interaction between FAM49B and NEK9 in SW480 cells by IF assay (E). After knocking down FAM49B, the expression of p-NEK9 (Thr210) and NEK9 in SW480 cells and SW620 cells was detected by western blot. (F) Western blot analysis of p-NEK9 (Thr210) and NEK9 expression in SW480 cells and SW620 cells with ectopic overexpression of FAM49B.

with stable FAM49B knockdown. The results showed that compared with the control group, FAM49B knockdown significantly inhibited the expression of c-Myc (Figure 5G). Conversely, overexpression of FAM49B can significantly up-regulate the expression of c-Myc (Figure 5H). However, the mRNA expression levels of c-Myc are not affected by the expression of FAM49B (Figure 5I). It is well known that c-Myc protein is mainly degraded by ubiquitin proteasome pathway,[36] and K48 ubiquitin is the main pathway of protein degradation. Consistently, the half-life of c-Myc protein was significantly reduced by stable knockdown of FAM49B (Figure 5J,K), and its degradation could be blocked by the proteasome inhibitor MG132 (Figure 5L,M). Moreover, c-Myc K48-linked ubiquitination levels increased significantly after FAM49B knockdown (Figure 5N). Therefore, FAM49B could be a potential stabilizer of c-Myc in CRC cells.

TABLE 2 IP-MS identification of 31 proteins with FAM49B possible interaction.

	IP-FAM49B			(Flag-FAM49B)IP-Flag		
Protein	**Log2FC (IP/IgG)**	**Sum PEP score**	**MW [kDa]**	**Log2FC (IP/IgG)**	**Sum PEP score**	**MW [kDa]**
NEK9	6.97	201.31	107.1	6.62	283.28	107.1
SERPINH1	4.71	128.91	46.4	5.81	243.35	46.4
CPSF3	6.18	63.97	77.4	5.71	78.88	77.4
PPIL2	4.62	73.85	58.8	5.42	128.27	58.8
CAPRIN1	5.12	117.13	78.3	5.41	147.90	78.3
SMARCC1	3.41	50.73	122.8	5.36	70.21	122.8
CPSF1	3.40	114.67	160.8	5.26	151.88	160.8
CPSF2	5.23	78.33	88.4	5.26	90.99	88.4
MATR3	3.65	113.33	94.6	4.72	169.46	94.6
COL1A1	3.33	65.14	138.9	4.55	141.71	138.9
PRRC2A	2.19	62.80	228.7	4.45	103.52	228.7
PABPC4	3.53	156.01	70.7	3.78	206.67	70.7
ASCC3	3.77	116.34	251.3	3.65	77.07	251.3
ATXN2L	2.13	61.48	113.3	3.53	115.98	113.3
SMARCA4	5.91	93.87	184.5	3.51	134.69	184.5
PABPC1	3.11	204.08	70.6	3.46	270.68	70.6
PTBP1	1.52	77.79	57.5	3.46	130.11	57.2
WDR33	4.81	62.83	145.8	3.37	133.11	145.8
NONO	1.87	60.82	54.2	3.29	103.66	54.2
RPS2	1.53	51.68	31.3	3.21	67.01	31.3
PLOD3	3.89	54.80	84.7	3.20	64.18	84.7
SFPQ	1.54	114.57	76.1	3.03	149.16	76.1
FXR1	1.61	94.41	69.7	2.85	134.69	69.7
RPS4X	1.58	65.60	29.6	2.80	71.94	29.6
LARP4	3.45	82.52	80.5	2.68	70.20	80.5
USP10	1.63	57.15	87.1	2.58	64.38	87.1
G3BP1	1.99	101.22	52.1	2.36	97.46	52.1
EIF3L	2.24	51.25	66.7	2.34	73.79	66.7
ANK1	5.14	111.4	206.1	2.33	66.31	206.1
SERBP1	1.74	86.70	44.9	2.22	114.05	44.9
RPL3	1.57	111.37	46.1	1.54	122.55	46.1

3.6 | NEK9 is the main intermediate molecule of FAM49B regulating c-Myc

To further determine whether FAM49B regulates the stability of c-Myc directly or indirectly, four protein hydrolysates were prepared, and corresponding electrophoresis strips were produced for the following setups: (i) SW480 cells treated with IgG (control group), (ii) SW480 cells with endogenous FAM49B, (iii) SW480 cells with ectopically overexpressed FAM49B (Flag-FAM49B) treated with IgG, and (iv) SW480 cells with FAM49B (Flag-FAM49B) treated with Flag. Both setups (ii) and (iv) were conducted in duplicate. The interactions among proteins were subsequently analyzed through immunoprecipitation-mass spectrometry (Figure 6A). Strict screening (log2FC > 1.5, sum PEP score > 50) was put in force and a total of 31 proteins were identified that may interact with FAM49B (Table 2), but c-Myc protein was not found, which indicated that FAM49B could not directly interact with c-Myc. Interestingly, the top 10 interacting proteins in endogenous FAM49B group and ectopic overexpression FAM49B group had high

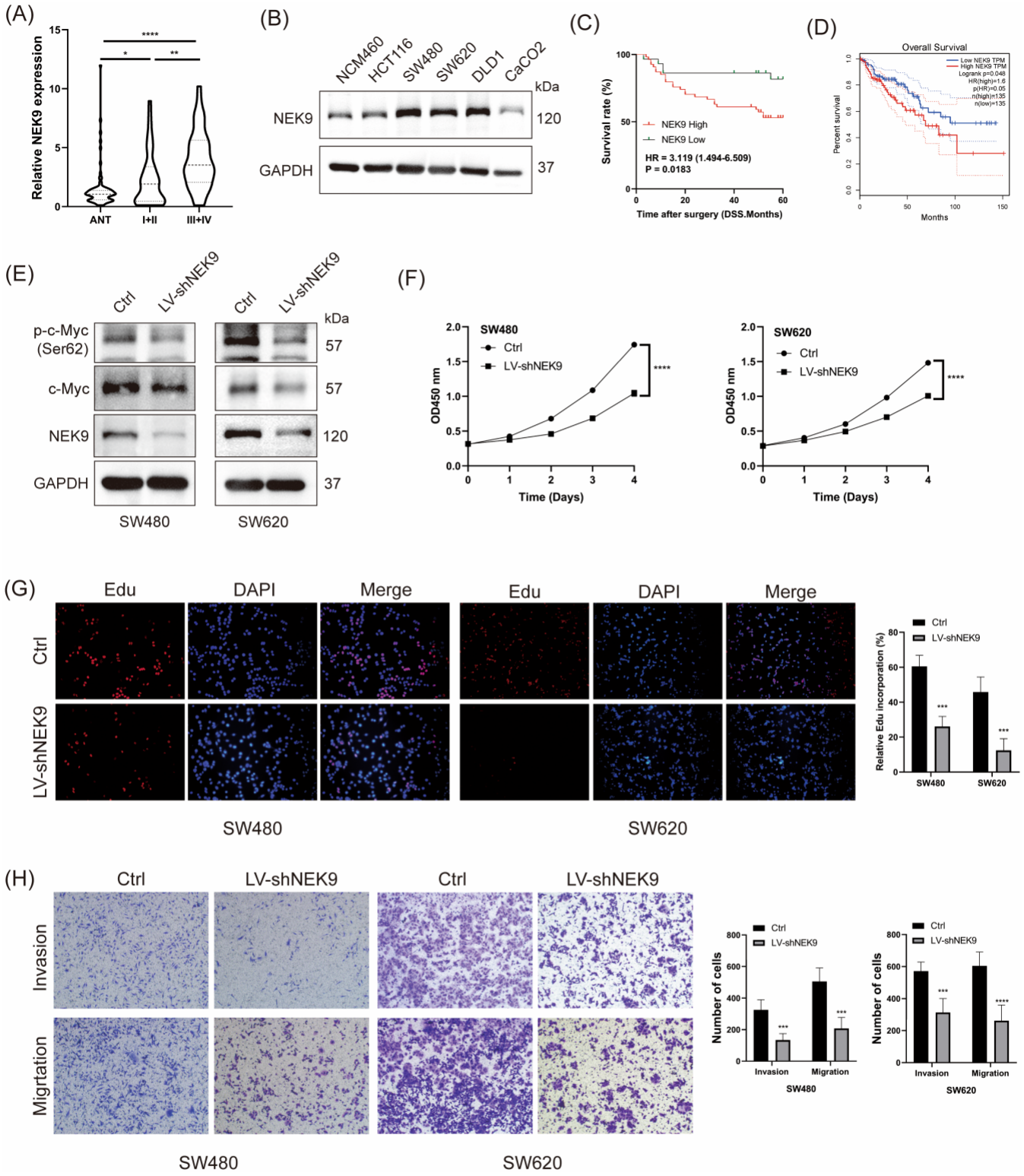

FIGURE 7 Legend on next page.

similarity. NEK9 protein ranked first in the two groups (Figure 6B). Moreover, NEK9 was the only kinase among the 31 proteins identified, which has the potential to activate c-Myc.

CO-IP and fluorescence co-localization experiments were used to confirm the interaction between FAM49B and NEK9. The results showed that FAM49B and NEK9 were bound in SW480 cells and SW620 cells (Figure 6C),

and the binding site was mainly in the cytoplasm (Figure 6D). In addition, through western blot detection, we found that the phosphorylation of NEK9-Thr210 in SW480 cells and SW620 cells was significantly weakened after FAM49B was knocked down (Figure 6E), while it was significantly enhanced after FAM49B was overexpressed (Figure 6F). Previous studies have shown that the increase in phosphorylation of NEK9-Thr210 is a sign of NEK9 activation,[37] which indicated that the activation of NEK9 requires FAM49B.

3.7 | NEK9 is related to poor prognosis of CRC patients and promotes CRC progression

The expression of NEK9 in colorectal cancer was significantly higher than that in adjacent tissues, and the higher the tumor stage, the higher the expression (Figure 7A). Furthermore, the expression of NEK9 protein in colorectal cancer cell lines (HCT116, SW480, SW620, and DLD1) was also significantly higher than that in the normal colon epithelial cell line NCM460 (Figure 7B). Subsequently, it was found that the higher the expression of NEK9, the worse the prognosis of patients (HR = 3.119, $p = 0.0183$, Figure 7C). In the GEPIA database, Kaplan–Meier survival analysis showed high NEK9 expression was a risk factor for OS of COAD (TCGA COAD, HR = 1.6, $p = 0.048$, Figure 7D).

To confirm whether NEK9 affects the function of CRC cells, we also designed three siRNA sequences to knock down the expression of NEK9. The results showed that # si-3 had the most significant knockdown efficiency (Figure S2A,B) and was made into the lentivirus. The proliferation, migration, and invasion functions of SW480 and SW620 cells were significantly inhibited after stably knocking down NEK9 (Figure 7F–H), while NEK9 overexpression promoted their proliferation, migration, and invasion (Figure S2C–E). Additionally, to determine whether NEK9 regulates the expression of c-Myc, or even promotes the phosphorylation of c-Myc, changes in the expression and phosphorylation of c-Myc at Ser62 site were analyzed using western blot after stable knockdown of NEK9 in SW480 and SW620 cells. Compared with the control group, the expression of c-Myc protein and the phosphorylation of c-Myc-Ser62 site were significantly inhibited in the NEK9 knockdown group (Figure 7E).

3.8 | FAM49B regulates c-Myc by activating NEK9 to promote CRC cell proliferation and migration

To clarify whether FAM49B regulates the expression and phosphorylation of c-Myc by activating NEK9, we manipulated NEK9 expression in CRC cells overexpressing FAM49B to determine changes in c-Myc expression and phosphorylation levels by western blot analysis. When FAM49B was overexpressed ectopically, the phosphorylation of NEK9-Thr210 was enhanced, and the expression of c-Myc protein and the phosphorylation of Ser62 were significantly up-regulated. Based on this, when the expression of NEK9 is knocked down, the phosphorylation of NEK9-Thr210 was almost completely inhibited, while the expression of c-Myc protein and the phosphorylation of Ser62 could be significantly reversed. When NEK9 was overexpressed, the phosphorylation of NEK9-Thr210 was more obvious, and the expression of c-Myc protein and the phosphorylation of Ser62 were significantly further enhanced (Figure 8A,B).

To better explore whether the FAM49B/NEK9/c-Myc axis could promote CRC progression, we further detected the proliferation, migration, and invasion ability of CRC cells. The results showed that the proliferation, migration, and invasion ability of cells were significantly enhanced after ectopic overexpression of FAM49B. Based on this, when the expression of NEK9 was knocked down, the proliferation, migration and invasion ability were significantly inhibited. When NEK9 was overexpressed, the proliferation, migration, and invasion ability were significantly further enhanced (Figure 8C–G). These

FIGURE 7 NEK9 is related to poor prognosis of CRC patients and promotes CRC cells proliferation, migration, and invasion. (A) Expression levels of NEK9 mRNA in colorectal cancer tissues and adjacent normal tissues. (B) Western blot analysis of NEK9 protein expression between normal colon epithelial cells and CRC cell lines. (C) Kaplan–Meier survival curve was used to compare the DSS survival time of 83 CRC patients in the NEK9 high expression group and the low expression group. (D) Kaplan–Meier survival curve was used to compare the OS survival time of CRC patients in the TCGA COAD dataset between the group with high NEK9 expression and the group with low NEK9 expression. (E) After knocking down NEK9, western blot assay was used to detect the expression changes of p-c-Myc (Ser62) and c-Myc in SW480 cells and SW620 cells. (F) After knocking down NEK9, the proliferation activity of SW480 (left) and SW620 (right) cells was detected by CCK-8. (G) The proliferation ability of SW480 and SW620 cells was detected by Edu assay and corresponding statistical analysis was performed. (H) The migration and invasion ability of SW480 and SW620 cells were detected by Transwell assay, and the corresponding statistical analysis was performed. The scale is 100 μm. ***$p < 0.001$, ****$p < 0.0001$.

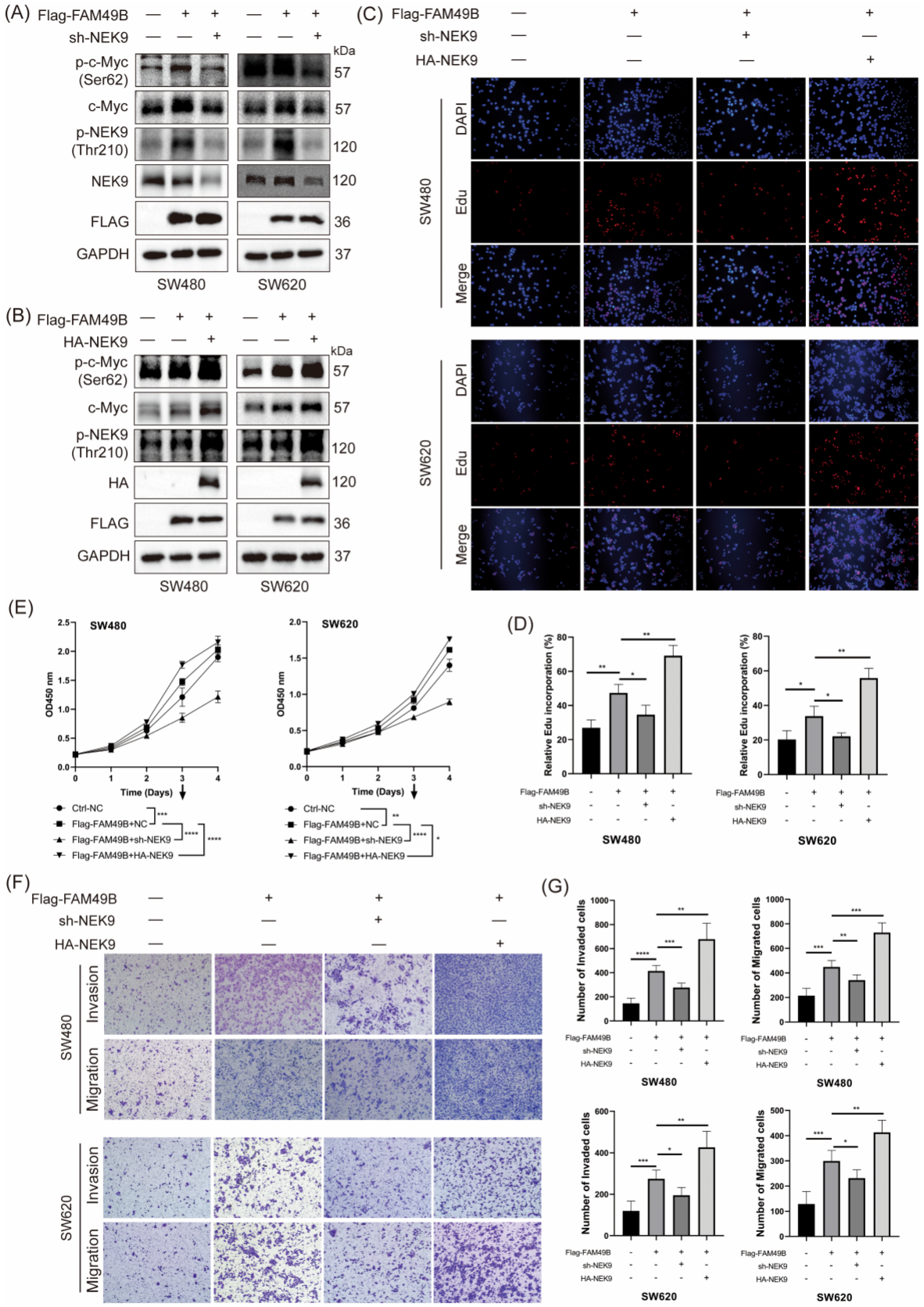

FIGURE 8 Legend on next page.

data show that the activation of the FAM49B/NEK9/c-Myc axis can promote CRC progression.

4 | DISCUSSION

Currently, comprehensive treatment strategies, including surgical resection, have proven effective in managing localized CRC. However, once colorectal cancer cells metastasize to distant organs, the disease progresses to a systemic condition, affecting multiple organs and making it more difficult to treat effectively.[38–41] This metastatic progression becomes a leading cause of mortality in CRC patients, highlighting the urgent need to further elucidate the underlying mechanisms of colorectal cancer development, progression, and metastasis.[42]

FAM49B, a member of the family with sequence similarity 49 (FAM49), is a recently discovered gene with evolutionarily conserved characteristics. Limited studies suggest that FAM49B may have critical tissue-specific roles, particularly in regulating cell movement. Recent research indicates that FAM49B is involved in tumor proliferation, invasion, and metastasis, though the specific mechanisms appear varied and sometimes contradictory.[43–46] Li et al. found that FAM49B promotes breast cancer proliferation, metastasis, and chemoresistance.[44] Zhang et al. discovered that FAM49B regulated by TASP1 promotes gallbladder cancer cell proliferation and metastasis.[8] But in pancreatic cancer, Chattaragada et al. identified FAM49B as a tumor suppressor.[43] Our study contributes to this growing body of knowledge by demonstrating that FAM49B expression is significantly elevated in CRC tissues and correlates with poor prognosis. These findings suggest that FAM49B could serve as a valuable prognostic biomarker, particularly for patients at high risk of metastatic disease.

In this study, we found that FAM49B expression is elevated in colorectal cancer and is significantly associated with poor prognosis. Functionally, FAM49B promotes proliferation, migration, and invasion in vitro, as well as metastasis in vivo, underscoring its potential role in colorectal cancer progression. Mechanistically, FAM49B phosphorylates, stabilizes, and activates c-Myc, largely by activating NEK9. Simply put, these three proteins assemble into a regulatory axis in CRC cells, serving as potential risk factors that promote the progression of CRC. In addition, these findings are closely associated with clinical prognostic outcomes. Both scRNA analysis from tissue samples and cellular level studies demonstrate a significant correlation between FAM49B and the activation of the oncogene c-Myc, which plays a crucial role in promoting CRC progression.[47] The correlation between FAM49B expression and c-Myc activation highlights the potential of FAM49B as a prognostic biomarker.

NEK9 (NIMA-related protein kinase 9) is a member of the NEK family of serine/threonine kinases that are emerging as important regulators of the cell cycle and checkpoint control.[48] Activated NEK9 phosphorylates NEK6 and NEK7, which in turn phosphorylate essential components such as Eg5, microtubules, and c-TuRC, crucial for the correct formation of the mitotic spindle.[48] Kinase activity is the core function of NEK9.[49] Foregone studies have confirmed that the increase of phosphorylation of NEK9-Thr210 is a sign of NEK9 activation.[37] Lu et al. discovered that NEK9, activated by SLIT2 derived from cancer-associated fibroblasts, and also activated by IL-6/STAT3, promotes metastasis of gastric cancer.[50,51] But in pancreatic cancer, NEK9 expression was downregulated in tumor tissues, and low NEK9 mRNA expression was related to poor overall survival.[52] However, the role of NEK9 in CRC remains poorly understood. In the context of CRC, we show that NEK9 activation, through phosphorylation at Thr210, plays a crucial role in stabilizing c-Myc and promoting tumor cell proliferation. Our findings suggest that NEK9 not only regulates mitotic processes but also acts as a key mediator of FAM49B-driven oncogenesis in CRC. Additionally, with the knock-down of NEK9 expression, the proliferation, migration, and invasion of CRC cells were significantly inhibited, the expression of c-Myc protein and the phosphorylation of c-Myc-Ser62 site was also significantly

FIGURE 8 FAM49B enhanced the expression of c-Myc protein and phosphorylated c-Myc (Ser62) by promoting the phosphorylation of NEK9-Thr210, which promoted the progression of CRC. (A) On the basis of ectopic overexpression of FAM49B, NEK9 was knocked down, and the expression changes of p-NEK9(Thr210), NEK9, p-c-Myc (Ser62), and c-Myc were detected by western blot. (B) On the basis of ectopic overexpression of FAM49B, NEK9 was overexpressed, and the expression changes of p-NEK9(Thr210), NEK9, p-c-Myc (Ser62), and c-Myc were detected by western blot. (C, D) The proliferation ability was examined by Edu assay in the Flag-FAM49B group transfected with NEK9 siRNA or NEK9 plasmid, and corresponding statistical analysis was performed. (E) The growth rate was detected by CCK-8 assay in the Flag-FAM49B group transfected with NEK9 siRNA or NEK9 plasmid. (F, G) The invasion and migration abilities were examined by Transwell assay in the Flag-FAM49B group transfected with NEK9 siRNA or NEK9 plasmid, and corresponding statistical analysis was performed. The scale is 100 μm. * < 0.05, **$p < 0.01$, *** < 0.001, ****$p < 0.0001$.

inhibited, which verified the relationship between NEK9 and c-Myc. Although our current evidence does not definitively show that NEK9 directly binds to c-Myc,[53,54] researchers have identified NEK9 in the protein interactome of c-Myc. This suggests that NEK9 is likely a direct kinase of c-Myc and acts as an intermediary between FAM49B and c-Myc.

In summary, our study is the first to demonstrate the clinical and biological significance of FAM49B and NEK9 in CRC, showing that the interaction between these two proteins stabilizes and activates the oncogene c-Myc, thereby facilitating CRC progression. Certainly, the details within this finding still require continual refinement. Overall, FAM49B can serve as a prognostic biomarker, and targeting FAM49B pharmacologically may offer a potential therapeutic approach for CRC patients.

AUTHOR CONTRIBUTIONS

Chen Lu: Writing—original draft; investigation; conduction; validation; visualization. **Tianyu Liu**: Investigation; software; data curation; formal analysis. **E. Yiming**: Methodology; data curation; formal analysis. **Lin Miao**: Data collection; visualization. **Chunzhao Yu**: Writing—review and editing; supervision; data curation. **Jianping Zhang**: Writing—review and editing; conceptualization; investigation. **Xiagang Luo**: Writing—original draft; investigation; supervision; resources; project administration.

ACKNOWLEDGMENTS

The mechanistic scheme of this study was drawn by Figdraw (https://www.figdraw.com).

FUNDING INFORMATION

This work was supported by Jiangsu Provincial Commission of Health and Family Planning (Z201603); Science and Technology Development Fund of Nanjing Health and Family Planning Commission (YKK16233); Youth talent support program of Nanjing City during the 13th Five-Year Plan Period (QRX17107).

CONFLICT OF INTEREST STATEMENT

The authors have no conflicts of interest to declare.

DATA AVAILABILITY STATEMENT

The data that support the findings of this study are available from the corresponding author upon reasonable request.

ORCID

Xiagang Luo https://orcid.org/0009-0009-0556-8379

REFERENCES

1. Bray F, Ferlay J, Soerjomataram I, Siegel RL, Torre LA, Jemal A. Global cancer statistics 2018: GLOBOCAN estimates of incidence and mortality worldwide for 36 cancers in 185 countries. CA Cancer J Clin. 2018;68:394–424.
2. Keller DS, Berho M, Perez RO, Wexner SD, Chand M. The multidisciplinary management of rectal cancer. Nat Rev Gastroenterol Hepatol. 2020;17:414–29.
3. Lai IL, You JF, Chern YJ, Tsai WS, Chiang JM, Hsieh PS, et al. The risk factors of local recurrence and distant metastasis on pT1/T2N0 mid-low rectal cancer after total mesorectal excision. World J Surg Oncol. 2021;19:116.
4. Chen Z, Borek D, Padrick SB, Gomez TS, Metlagel Z, Ismail AM, et al. Structure and control of the actin regulatory WAVE complex. Nature. 2010;468:533–8.
5. Fort L, Batista JM, Thomason PA, Spence HJ, Whitelaw JA, Tweedy L, et al. Fam49/CYRI interacts with Rac1 and locally suppresses protrusions. Nat Cell Biol. 2018;20:1159–71.
6. Gilli F, Navone ND, Perga S, Marnetto F, Caldano M, Capobianco M, et al. Loss of braking signals during inflammation: a factor affecting the development and disease course of multiple sclerosis. Arch Neurol. 2011;68:879–88.
7. Nagarajan NA, Gonzalez F, Shastri N. Nonclassical MHC class Ib-restricted cytotoxic T cells monitor antigen processing in the endoplasmic reticulum. Nat Immunol. 2012;13:579–86.
8. Zhang Y, Du P, Li Y, Zhu Q, Song X, Liu S, et al. TASP1 promotes gallbladder cancer cell proliferation and metastasis by up-regulating FAM49B via PI3K/AKT pathway. Int J Biol Sci. 2020;16:739–51.
9. Chen Y, Jiang Y, Lao J, Zhou Y, Su L, Huang X. Characterization and functional study of FAM49B reveals its effect on cell proliferation in HEK293T cells. Genes (Basel). 2022;13:388–402.
10. Ellwood-Yen K, Graeber TG, Wongvipat J, Iruela-Arispe ML, Zhang J, Matusik R, et al. Myc-driven murine prostate cancer shares molecular features with human prostate tumors. Cancer Cell. 2003;4:223–38.
11. Kim J, Roh M, Doubinskaia I, Algarroba GN, Eltoum IE, Abdulkadir SA. A mouse model of heterogeneous, c-MYC-initiated prostate cancer with loss of Pten and p53. Oncogene. 2012;31:322–32.
12. Kim HY, Kim YM, Hong S. Astaxanthin suppresses the metastasis of colon cancer by inhibiting the MYC-mediated downregulation of microRNA-29a-3p and microRNA-200a. Sci Rep. 2019;9:9457.
13. Tanaka T, Kaida T, Yokoi K, Ishii S, Nishizawa N, Kawamata H, et al. Critical relevance of genomic gains of PRL-3/EGFR/c-myc pathway genes in liver metastasis of colorectal cancer. Oncol Lett. 2019;17:1257–66.
14. Shan L, Zheng W, Bai B, Hu J, Lv Y, Chen K, et al. BMAL1 promotes colorectal cancer cell migration and invasion through ERK- and JNK-dependent c-Myc expression. Cancer Med. 2023;12:4472–85.
15. Napoli S, Pastori C, Magistri M, Carbone GM, Catapano CV. Promoter-specific transcriptional interference and c-myc gene silencing by siRNAs in human cells. EMBO J. 2009;28:1708–19.

16. Benassi B, Flavin R, Marchionni L, Zanata S, Pan Y, Chowdhury D, et al. MYC is activated by USP2a-mediated modulation of microRNAs in prostate cancer. Cancer Discov. 2012;2:236–47.
17. Ciccarelli C, Di Rocco A, Gravina GL, Mauro A, Festuccia C, Del Fattore A, et al. Disruption of MEK/ERK/c-Myc signaling radiosensitizes prostate cancer cells in vitro and in vivo. J Cancer Res Clin Oncol. 2018;144:1685–99.
18. Zhang Y, Wang Z, Li X, Magnuson NS. Pim kinase-dependent inhibition of c-Myc degradation. Oncogene. 2008;27:4809–19.
19. Kalkat M, Resetca D, Lourenco C, Chan PK, Wei Y, Shiah YJ, et al. MYC protein interactome profiling reveals functionally distinct regions that cooperate to drive tumorigenesis. Mol Cell. 2018;72:836–48.
20. Nowak DG, Cho H, Herzka T, Watrud K, DeMarco DV, Wang VM, et al. MYC drives Pten/Trp53-deficient proliferation and metastasis due to IL6 secretion and AKT suppression via PHLPP2. Cancer Discov. 2015;5:636–51.
21. Lin X, Sun R, Zhao X, Zhu D, Zhao X, Gu Q, et al. C-myc overexpression drives melanoma metastasis by promoting vasculogenic mimicry via c-myc/snail/Bax signaling. J Mol Med (Berl). 2017;95:53–67.
22. Lee HY, Cha J, Kim SK, Park JH, Song KH, Kim P, et al. c-MYC drives breast cancer metastasis to the brain, but promotes synthetic lethality with TRAIL. Mol Cancer Res. 2019;17:544–54.
23. Arriaga JM, Panja S, Alshalalfa M, Zhao J, Zou M, Giacobbe A, et al. A MYC and RAS co-activation signature in localized prostate cancer drives bone metastasis and castration resistance. Nat Can. 2020;1:1082–96.
24. Klotz R, Thomas A, Teng T, Han SM, Iriondo O, Li L, et al. Circulating tumor cells exhibit metastatic tropism and reveal brain metastasis drivers. Cancer Discov. 2020;10:86–103.
25. Adams JA. Kinetic and catalytic mechanisms of protein kinases. Chem Rev. 2001;101:2271–90.
26. Duong-Ly KC, Peterson JR. The human kinome and kinase inhibition. Curr Protoc Pharmacol. 2013;60:2.9.1–14.
27. Sears R, Nuckolls F, Haura E, Taya Y, Tamai K, Nevins JR. Multiple Ras-dependent phosphorylation pathways regulate Myc protein stability. Genes Dev. 2000;14:2501–14.
28. Farrell AS, Sears RC. MYC degradation. Cold Spring Harb Perspect Med. 2014;4:a014365.
29. Devaiah BN, Mu J, Akman B, Uppal S, Weissman JD, Cheng D, et al. MYC protein stability is negatively regulated by BRD4. Proc Natl Acad Sci USA. 2020;117:13457–67.
30. Tang Z, Li C, Kang B, Gao G, Li C, Zhang Z. GEPIA: a web server for cancer and normal gene expression profiling and interactive analyses. Nucleic Acids Res. 2017;45:W98–W102.
31. Hao Y, Hao S, Andersen-Nissen E, Mauck WM 3rd, Zheng S, Butler A, et al. Integrated analysis of multimodal single-cell data. Cell. 2021;184:3573–87.
32. McGinnis CS, Murrow LM, Gartner ZJ. DoubletFinder: doublet detection in single-cell RNA sequencing data using artificial nearest neighbors. Cell Syst. 2019;8:329–37.
33. Korsunsky I, Millard N, Fan J, Slowikowski K, Zhang F, Wei K, et al. Fast, sensitive and accurate integration of single-cell data with harmony. Nat Methods. 2019;16:1289–96.
34. Tirosh I, Izar B, Prakadan SM, Wadsworth MH 2nd, Treacy D, Trombetta JJ, et al. Dissecting the multicellular ecosystem of metastatic melanoma by single-cell RNA-seq. Science. 2016;352:189–96.
35. Gu J, Zhou P, Liu Y, Xu Q, Chen X, Chen M, et al. Down-regulating interleukin-22/interleukin-22 binding protein axis promotes inflammation and aggravates diet-induced metabolic disorders. Mol Cell Endocrinol. 2022;557:111776.
36. Sammak S, Hamdani N, Gorrec F, Allen MD, Freund SMV, Bycroft M, et al. Crystal structures and nuclear magnetic resonance studies of the Apo form of the c-MYC:MAX bHLHZip complex reveal a helical basic region in the absence of DNA. Biochemistry. 2019;58:3144–54.
37. Levinsohn JL, Sugarman JL, G. Yale Center for Mendelian, McNiff JM, Antaya RJ, Choate KA. Somatic mutations in NEK9 cause nevus comedonicus. Am J Hum Genet. 2016;98:1030–7.
38. Carlomagno C, De Stefano A, Rosanova M, De Falco S, Attademo L, Fiore G, et al. Multiple treatment lines and prognosis in metastatic colorectal cancer patients. Cancer Metastasis Rev. 2019;38:307–13.
39. Piawah S, Venook AP. Targeted therapy for colorectal cancer metastases: A review of current methods of molecularly targeted therapy and the use of tumor biomarkers in the treatment of metastatic colorectal cancer. Cancer. 2019;125:4139–47.
40. Welch DR, Hurst DR. Defining the hallmarks of metastasis. Cancer Res. 2019;79:3011–27.
41. Massague J, Ganesh K. Metastasis-initiating cells and ecosystems. Cancer Discov. 2021;11:971–94.
42. Dekker E, Tanis PJ, Vleugels JLA, Kasi PM, Wallace MB. Colorectal cancer. Lancet. 2019;394:1467–80.
43. Chattaragada MS, Riganti C, Sassoe M, Principe M, Santamorena MM, Roux C, et al. FAM49B, a novel regulator of mitochondrial function and integrity that suppresses tumor metastasis. Oncogene. 2018;37:697–709.
44. Li Y, Xiong Y, Wang Z, Han J, Shi S, He J, et al. FAM49B promotes breast cancer proliferation, metastasis, and chemoresistance by stabilizing ELAVL1 protein and regulating downstream Rab10/TLR4 pathway. Cancer Cell Int. 2021;21:534.
45. Pereira BS, Wisnieski F, Calcagno DQ, Santos LC, Gigek CO, Chen ES, et al. Genetic and transcriptional analysis of 8q24.21 cluster in gastric cancer. Anticancer Res. 2022;42:4381–94.
46. Xu F, Chen J, Huang D. Pan-cancer analysis identifies FAM49B as an immune-related prognostic maker for hepatocellular carcinoma. J Cancer. 2022;13:278–89.
47. Ying Y, Wang Y, Huang X, Sun Y, Zhang J, Li M, et al. Oncogenic HOXB8 is driven by MYC-regulated super-enhancer and potentiates colorectal cancer invasiveness via BACH1. Oncogene. 2020;39:1004–17.
48. Fry AM, O'Regan L, Sabir SR, Bayliss R. Cell cycle regulation by the NEK family of protein kinases. J Cell Sci. 2012;125:4423–33.
49. van de Kooij B, Creixell P, van Vlimmeren A, Joughin BA, Miller CJ, Haider N, et al. Comprehensive substrate specificity profiling of the human Nek kinome reveals unexpected signaling outputs. elife. 2019;8:e44635.
50. Lu G, Tian S, Sun Y, Dong J, Wang N, Zeng J, et al. NEK9, a novel effector of IL-6/STAT3, regulates metastasis of gastric cancer by targeting ARHGEF2 phosphorylation. Theranostics. 2021;11:2460–74.

51. Lu G, Du R, Dong J, Sun Y, Zhou F, Feng F, et al. Cancer associated fibroblast derived SLIT2 drives gastric cancer cell metastasis by activating NEK9. Cell Death Dis. 2023;14:421.
52. Nie H, Huang PQ, Jiang SH, Yang Q, Hu LP, Yang XM, et al. The short isoform of PRLR suppresses the pentose phosphate pathway and nucleotide synthesis through the NEK9-Hippo axis in pancreatic cancer. Theranostics. 2021;11:3898–915.
53. Koch HB, Zhang R, Verdoodt B, Bailey A, Zhang CD, Yates JR 3rd, et al. Large-scale identification of c-MYC-associated proteins using a combined TAP/MudPIT approach. Cell Cycle. 2007;6:205–17.
54. Heidelberger JB, Voigt A, Borisova ME, Petrosino G, Ruf S, Wagner SA, et al. Proteomic profiling of VCP substrates links VCP to K6-linked ubiquitylation and c-Myc function. EMBO Rep. 2018;19:e44754.

SUPPORTING INFORMATION

Additional supporting information can be found online in the Supporting Information section at the end of this article.

How to cite this article: Lu C, Liu T, Yimin E, Miao L, Yu C, Zhang J, et al. FAM49B drives colorectal cancer progression by stabilizing c-Myc through NEK9 phosphorylation. BioFactors. 2025; 51(1):e2158. https://doi.org/10.1002/biof.2158